Chapter 7

Sum Rules Associated with Non-singlet Structure Functions

In this chapter, we have determined the three sum rules viz., the Gottfired Sum rule(GSR), the Gross-Llewellyn Smith sum rule(GLSSR) and the Bjorken sum rule(BSR), which are associated with the non-singlet structure functions F_2^{NS}, xF_3 and xg_1^{NS} respectively with QCD corrections up to NNLO. The determination of sum rules requires the knowledge of structure functions only at small-x and these requirements are obtained from the previous chapters, where we have successfully evolved the non-singlet structure functions in accord with DGLAP equation through an approach unifying Regge theory and pQCD. We have also perform a phenomenological analysis of our results for various sum rules in comparison with their respective experimental and parametrization results.

7.1 Introduction

Deep inelastic structure functions obey a series of Sum rules, which are integrals over structure functions or parton distributions, expressing usually the conservation law for some quantum number of the nucleon. These sum rules provide information about the distribution of quarks inside nucleon and are very useful to reveal new physics if a sum rule is observed to be satisfied or broken. Perturbative Quantum Chromodynamics has predictions of a wide variety sum rules and they are expected to provide us with a stringent test of QCD. Because, the sum rules are expressed as the integrals of the form $\int_0^1 dx F(x, Q^2) = A$, and in this representation, one gets rid of the unknown x-dependence which is due to non-perturbative effects. Further, sum

rules can be computed up to much higher orders in perturbative QCD than other quantities. Therefore the sum rules have been the subject of great experimental, theoretical as well as phenomenological investigation.

In order to investigate the validity of QCD as a theory of strong interaction by means of sum rules, many successful experimental programs of both polarized and unpolarized deep-inelastic lepton nucleon scattering have been performed. With the advent of dedicated experimental facilities the recent measurements of the structure functions of both polarized and un-polarized DIS[7] in the wide interval of the $x = \frac{Q^2}{2pq}$ variable open the possibility of a more precise determination of the number of the DIS sum rules. In view of this experimental progress the detailed studies of the theoretical predictions for the DIS sum rules started to attract special attention.

Brief overview of the basic parton model sum rules have already been given in section 1.5 and commented on the status of their available QCD corrections. QCD corrections to sum rules mainly fall into two classes; those that are strongly suppressed at high energy (higher twist corrections) and those that vanish only logarithmically with the momentum transfer. The latter are fully calculable in terms of the coupling constant α_s of QCD.

The determination of these sum rules requires knowledge of the corresponding structure functions over the entire region of $x \in (0; 1)$. The experimentally accessible x range for the lepton DIS is however limited for the available data and therefore one should extrapolate results to $x = 0$ and $x = 1$. The extrapolation to $x \to 0$, where structure functions $\frac{1}{x}F_2^{NS}$, F_3 and g_1^{NS} grow strongly, is much more important than the extrapolation to $x \to 1$, where structure functions vanish. Again, it is known that maximum contribution (about 90%) to the GSR, GLSSR and BSR come from the small $x(\leq 0.1)$ region. Because of the large contribution to these sum rules from small x, the small x region is particularly important. In the following sections we will observe that the determination of sum rules requires the knowledge of structure functions only at small-x and the requirements are obtained from the previous chapters, where we have successfully evolved the non-singlet structure functions in accord with DGLAP equation through a unified approach unifying Regge theory and pQCD.

This chapter is divided into six sections. In the next section 7.2, we have presented a generalized formalism which is adopted in the determination of various sum rules. Then the same formalism is extended to incorporate the sum rules, GSR, GLSSR and BSR in the section 7.3, 7.4 and 7.5 respectively. In the respective sections we have

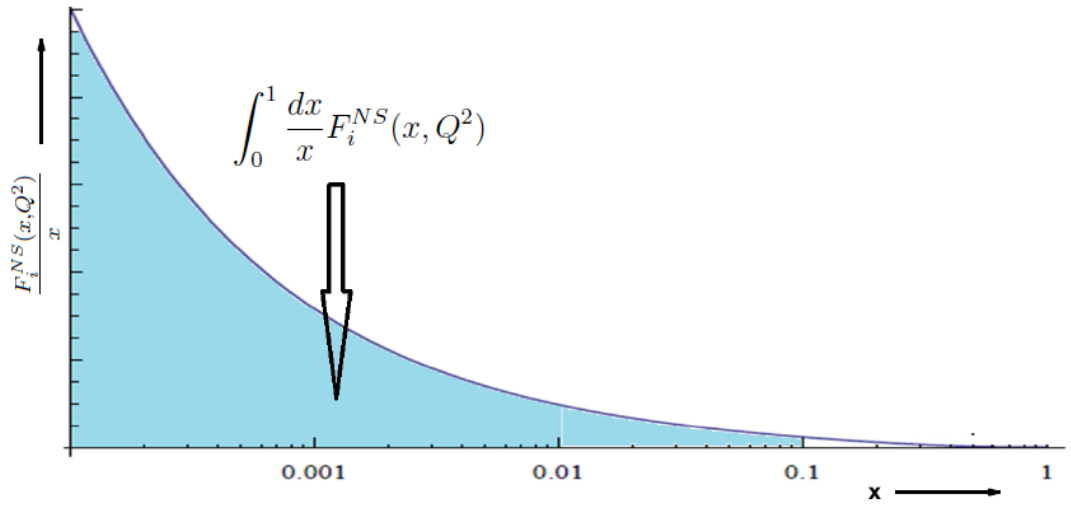

Figure 7.1: General interpretation of sum rule. The curve represents the variation of the structure function F_i^{NS} with x and the area under the curve represents the sum rule.

also provided a detailed analysis of our results for the sum rules in comparison with other available experimental and parametrization results. In the last section 7.6, the works performed and results obtained in this chapter are summarised.

7.2 The General Strategy Adopted in Determining Sum Rules

Away from $Q^2 \to \infty$, the Sum Rules, GSR, GLSSR and BSR are expressed in terms of a sum of two series in powers of the strong coupling constant $\alpha_s(Q^2)$ (leading twist pQCD correction)and in powers of $\frac{1}{Q^2}$(nonperturbative higher twist corrections):

$$S_i(Q^2) = \int_0^1 \frac{dx}{x} F_i^{NS}(x,Q^2) = S_i^{pQCD} + \sum_{i=2}^{\infty} \frac{\mu_{2i}^{p-n}(Q^2)}{Q^{2i-2}}, \tag{7.1}$$

where S_i denotes the sum rules associated with $F_i^{NS} = F_2^{NS}, xF_3, xg_1^{NS}$. Here the leading twist term (bracket term) consists of pQCD results and the second term on the r.h.s. is known as higher twist term. The higher order pQCD corrections and higher twist power corrections are significant at low-Q^2 region(see Ref. [163, 164] and references therein). In this chapter we have paid attention to only the first part i.e., the pQCD corrected term, S_i^{pQCD}.

In general the integral associated with the sum rules represents the area under the curve $F_i^{NS}(x,Q^2)$ from $x = 0$ to $x = 1$ (Shown in Fig. 7.1), which can be resolved

as

$$S_i(Q^2) = \int_0^{x_{min}} \frac{F_i^{NS}(x,Q^2)}{x}dx + \int_{x_{min}}^1 \frac{F_i^{NS}(x,Q^2)}{x}dx \tag{7.2}$$

and it gives

$$S_i(x_{min},Q^2) = \int_{x_{min}}^1 \frac{F_i^{NS}(x,Q^2)}{x}dx = S_i(Q^2) - \int_0^{x_{min}} \frac{F_i^{NS}(x,Q^2)}{x}dx. \tag{7.3}$$

The integral on the left hand side of (7.3) represents the area under the curve $\frac{F_i^{NS}(x,Q^2)}{x}$ from $x = x_{min}$ to $x = 1$. For $x = x_{min} \to 0$, this integral will tend to cover the whole area under the curve from $x = x_{min} = 0$ to $x = 1$, that is, it will represent the whole integral associated with the sum rule. Again the second part on the right side of (7.3) represents the part of total area $\int_0^1 \frac{F_i^{NS}(x,Q^2)}{x}dx$, laying under the curve $\frac{F_i^{NS}(x,Q^2)}{x}$ within smaller x region i.e., from $x = 0$ to any smaller value $x = x_{min}$. Thus we see that in order to investigate the sum rules, we just require the knowledge of corresponding structure function $F_i^{NS}(x,Q^2)$ within smaller x region. This requirement can be fulfilled by using the solutions of DGLAP equations obtained in our previous chapters.

Based on this general formalism, in the following sections we have investigated the GSR, GLSSR and BSR with pQCD corrections up to NNLO utilising the well behaved solutions of the DGLAP evolution equations for F_2^{NS}, xF_3 and xg_1^{NS} obtained in the previous chapters 4, 5 and 6 respectively.

7.3 Determination of Gottfried Sum Rule

The Gottfried Sum Rule(GSR)[34] is associated with the non-singlet structure function $F_2^{ep} - F_2^{en}$, the difference of F_2 measured on proton and on neutron in charged lepton scattering. In accord with parton model this sum rule expresses the fact that there is one more u valence quark than d valence quark in the proton and is only valid under the assumption that the seas of u and d quarks in the proton are equal($\bar{u} = \bar{d}$). It is written as

$$S_{GSR}(Q^2) = \int_0^1 \frac{dx}{x}\left[F_2^{ep}(x,Q^2) - F_2^{en}(x,Q^2)\right]$$
$$= \int_0^1 dx\left[\frac{1}{3}(u_v(x,Q^2) - d_v(x,Q^2)) + \frac{2}{3}(\bar{u}(x,Q^2) - \bar{d}(x,Q^2))\right]$$
$$= \frac{1}{3} + \frac{2}{3}\int_0^1 \left[\bar{u}(x,Q^2) - \bar{d}(x,Q^2)\right]dx. \tag{7.4}$$

In fact if the sea were flavour symmetric, namely $\bar{u} = \bar{d}$, we expect

$$S_{GSR} = \frac{1}{3}. \tag{7.5}$$

However, the most detailed analysis of muon-nucleon DIS data of NMC Collaboration gives the following result[65]

$$S_{GSR}(Q^2 = 4GeV^2) = 0.235 \pm 0.026, \tag{7.6}$$

which in turn indicates the violation of theoretical expression of Eq. 7.5 and necessitates more detailed investigations of different effects, related to the Gottfried sum rule.

In QCD, the leading twist pQCD correction up to NNLO for GSR is expressed as a series in powers of the strong coupling constant $\alpha_s(Q^2)$[35] :

$$S_{GSR}(Q^2) = \int_0^1 \frac{dx}{x}F_2^{NS}(x,Q^2) = \frac{1}{3}\left[1 + 0.0355\frac{\alpha_s}{\pi} - 0.811\left(\frac{\alpha_s}{\pi}\right)^2\right]. \tag{7.7}$$

Here the GSR consists of pQCD results up to second order of $\alpha_s(Q^2)$.

In accord with Eq. 7.3, the GSR integral can be represented as

$$S_{GSR}(x_{min},Q^2) = \int_{x_{min}}^1 \frac{F_2^{NS}(x,Q^2)}{x}dx = S_{GSR}(Q^2) - \int_0^{x_{min}} \frac{xg_1^{NS}(x,Q^2)}{x}dx. \tag{7.8}$$

From Eq. 7.8, it is clear that in order to calculate the integral on the l.h.s., which represents the GSR for $x_{min} \to 0$ limite, we need to know $F_2^{NS}(x,Q^2)$ structure function within smaller x region. This requirement can be fulfilled by using the solutions of DGLAP equations for F_2^{NS}, obtained in the chapter 4, which provide well description of the small-x behaviour of $F_2^{NS}(x,Q^2)$ structure function. Therefore, substituting (4.49), (4.50) and (4.51) in (7.8) (although the expressions (4.31)-(4.33))

and using the corresponding expressions for S_{GSR} in LO, NLO and NNLO, we obtain the GSR integral with LO, NLO and NNLO pQCD corrections as

$$S_{GSR}(x_{min},Q^2)\Big|_{LO} = S_{GSR}(Q^2)\Big|_{LO} - \int_0^{x_{min}} \frac{dx}{x}\Bigg[F_2^{NS}(x_0,t_0) \left(\frac{x}{x_0}\right)^{(1-bt)} \exp\Bigg\{\int_{t_0}^{t}\left(\frac{\alpha(t)}{2\pi}\right)_{LO} P(x_0,t)dt\Bigg\}\Bigg], \tag{7.9}$$

$$S_{GSR}(x_{min},Q^2)\Big|_{NLO} = S_{GSR}(Q^2)\Big|_{NLO} - \int_0^{x_{min}} \frac{dx}{x}\Bigg[F_2^{NS}(x_0,t_0) \left(\frac{x}{x_0}\right)^{(1-bt)} \exp\Bigg\{\int_{t_0}^{t}\left(\frac{\alpha(t)}{2\pi}\right)_{NLO} P(x_0,t)dt + \int_{t_0}^{t}\left(\frac{\alpha(t)}{2\pi}\right)^2_{NLO} Q(x_0,t)dt\Bigg\}\Bigg] \tag{7.10}$$

and

$$S_{GSR}(x_{min},Q^2)\Big|_{NNLO} = S_{GSR}(Q^2)\Big|_{NNLO} - \int_0^{x_{min}} \frac{dx}{x}\Bigg[F_2^{NS}(x_0,t_0)\left(\frac{x}{x_0}\right)^{(1-bt)} \exp\Bigg\{\int_{t_0}^{t}\left(\frac{\alpha(t)}{2\pi}\right)_{NNLO} P(x_0,t)dt + \int_{t_0}^{t}\left(\frac{\alpha(t)}{2\pi}\right)^2_{NNLO} Q(x_0,t)dt + \int_{t_0}^{t}\left(\frac{\alpha(t)}{2\pi}\right)^3_{NNLO} R(x_0,t)dt\Bigg\}\Bigg] \tag{7.11}$$

respectively. Considering a known input point $F_2^{NS}(x_0,t_0)$ from experimental data, we will be able to calculate the GSR integral up to NNLO corrections using the expressions, (7.9), (7.10) and (7.11) respectively.

In our calculation of GSR, we have used the NMC[63] experimental data point, $F_2^{NS}(x_0,t_0) = 0.010348 \pm 0.006208$ at $x_0 = 0.025$ and $Q^2 = 2.34686 GeV^2$ as the input point. With this input point we have calculated the Gottfired Sum rule and the results in accord with equations (7.9), (7.10) and (7.11) are depicted in Fig. 7.2 and Fig. 7.3 as a function of Q^2 in comparison with the results predicted by QCD in accord with Eq.(7.7).

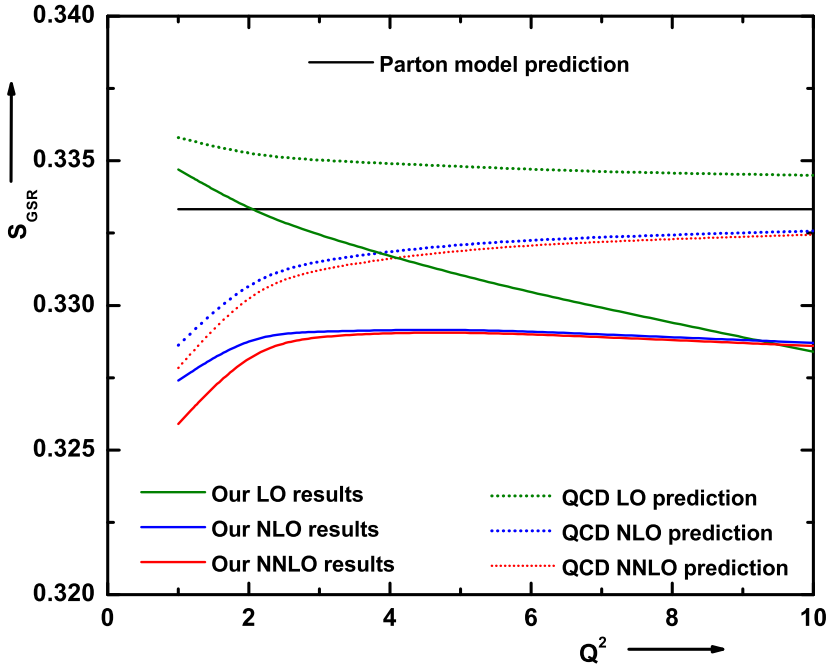

Figure 7.2: LO, NLO and NNLO results for GSR along with parton model and pQCD predictions. (Q^2's are taken in the unit of GeV^2).

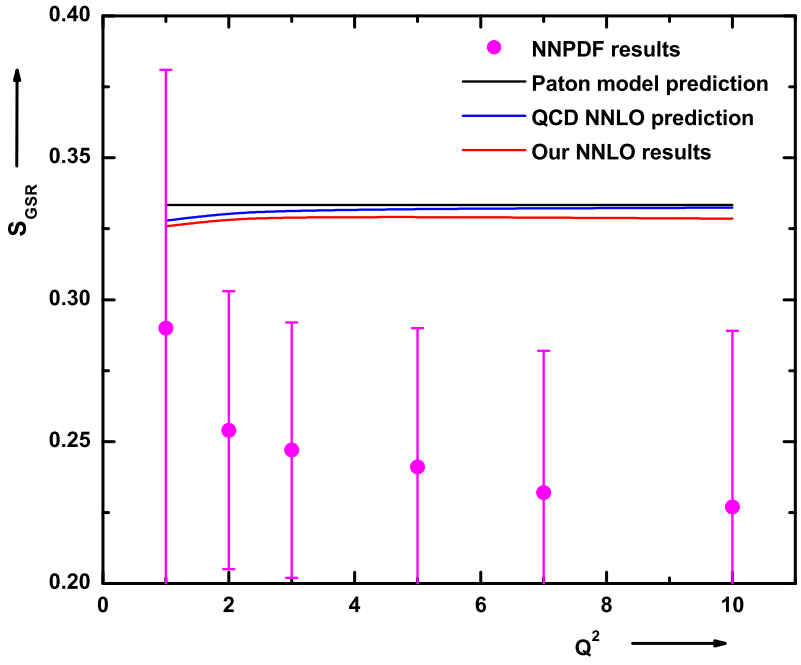

Figure 7.3: Our NNLO results for GSR in comparison with parton model and NNLO pQCD predictions as well as the results of NNPDF collaboration. (Q^2's are taken in the unit of GeV^2).

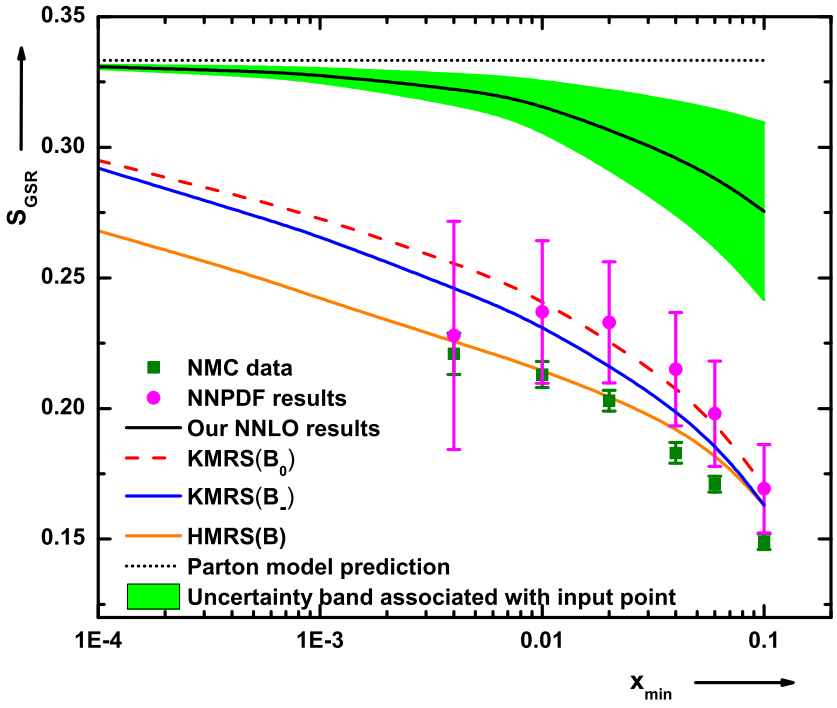

Figure 7.4: GSR as a function of x_{min} in comparison with NMC, NNPDF and KMRS results. The uncertainty band shown here is the uncertainty associated with the iput point.

In Fig. 7.3, the NNLO results are compared with the NNPDF[101] results. In Fig. 7.4 our results for GSR are depicted as a function of low x limit of integration x_{min} in comparison with those obtained by NMC, NNPDF and KMRS. Here we have also shown the estimated uncertainty band associated with the chosen input point. Although our result for GSR, as far the figures 7.2, 7.3 and 7.4 are concerned, do not agree well with those of NMC, NNPDF as well as KMRS, however a very good agreement with pQCD predictions is observed.

7.4 Determination of Gross-Llewellyn Smith Sum Rule

The Gross-Llewellyn Smith(GLS) sum rule[38, 39] associated with the non-singlet $xF_3(x, Q^2)$ structure function measured in neutrino-nucleon $(\nu - N)$ scattering is one of the best observables to investigate Quantum Chromodynamics(QCD) as a theory of strong interaction. Perturbative Quantum Chromodynamics (pQCD) predicts the value of the GLS integral up to next-next-to-leading order(NNLO) as a function of

strong coupling constant(α_s), the four momentum transfer(Q^2) and the number of accessible quark flavour (n_f). Up to NNLO pQCD corrections, the GLS integral can be written as[39]

$$S_{GLS}(Q^2) = \int_0^1 \frac{dx}{x} xF_3(x,Q^2) = 3\left[1 - \frac{\alpha_s}{\pi} - a(n_f)\left(\frac{\alpha_s}{\pi}\right)^2 - b(n_f)\left(\frac{\alpha_s}{\pi}\right)^3\right], \quad (7.12)$$

where the flavour dependent functions are given by $a(n_f) = \frac{55}{12} - \frac{n_f}{3}$ and $b(n_f) = 41.441 - 8.02n_f + 0.177n_f^2$.

As $xF_3(x,Q^2)$ structure function is not marred by the presence of the sea quark and gluon densities about which we have very poor information in particular in the small-x region and higher order QCD calculations are observed to be largely independent of renormalization scheme [165], this prediction is considered as the robust prediction in pQCD. In order to verify the GLS sum rule, experiments have been performed by CCFR collaboration[166] and obtained a precision of roughly 3% in accordance with the analysis in Ref. [167], using a leading-order(LO) QCD-based fit to extrapolate all data to $Q^2 = 3.2GeV^2$. However, some small but important corrections due to quark mass thresholds, target mass or higher twist effects, which were not included in previous analysis were reported in Ref. [165, 168–172]. In addition to these, some small but significant corrections arising from strange quark distributions and from charge symmetry violating parton distributions were also investigated recently in Ref. [173]. However, in this chapter we have focused only on the pQCD corrections up to NNLO.

In order to determine GLS sum rule we have adopted the similar formalism used in determining GSR. Here firstly we have resolved the GLS integral as

$$S_{GLS}(Q^2) = \int_0^{x_{min}} \frac{xF_3(x,Q^2)}{x} dx + \int_{x_{min}}^1 \frac{xF_3(x,Q^2)}{x} dx, \quad (7.13)$$

which gives

$$S_{GLS}(x_{min},Q^2) = \int_{x_{min}}^1 \frac{xF_3(x,Q^2)}{x} dx = S_{GLS}(Q^2) - \int_0^{x_{min}} \frac{xF_3(x,Q^2)}{x} dx. \quad (7.14)$$

The integral on the left hand side of (7.14) similarly represents the area under the curve $\frac{xF_3(x,Q^2)}{x}$ from $x = x_{min}$ to $x = 1$. For $x = x_{min} \to 0$, this integral will tend to cover the whole area under the curve from $x = x_{min} = 0$ to $x = 1$, that is, it will represent the GLS integral. Again the second part on the right side of (7.14) represents

the part of total area lying under the curve, $\frac{xF_3(x,Q^2)}{x}$ within smaller x region i.e., from $x = 0$ to any smaller value $x = x_{min}$. Thus we see that in order to investigate the GLS integral, we just require the knowledge of $xF_3(x, Q^2)$ structure function within smaller x region, not the entire region.

We have already obtained the small-x behaviour of $xF_3(x, Q^2)$ structure function by means of solving DGLAP evolution equation in chapter 5 and they are observed to be consistent with other experimental as well as parametrization results. Which implies that the analytical expressions, we have obtained in chapter 5 for $xF_3(x, Q^2)$ are applicable in describing small x behaviour of $xF_3(x, Q^2)$ structure function with a considerable precision and therefore those expressions can be successfully incorporated in $\int_0^{x_{min}} \frac{xF_3(x,Q^2)}{x} dx$ for $xF_3(x, Q^2)$ term and hence we can obtain the GLS integral (7.14) with LO, NLO and NNLO corrections as

$$S_{GLS}(x_{min}, Q^2)\Big|_{LO} = S_{GLS}(Q^2)\Big|_{LO} - \int_0^{x_{min}} \frac{dx}{x}\left[F_3^{NS}(x_0, t_0)\left(\frac{x}{x_0}\right)^{(1-bt)} \exp\left\{\int_{t_0}^{t}\left(\frac{\alpha(t)}{2\pi}\right)_{LO} P(x_0, t)dt\right\}\right], \quad (7.15)$$

$$S_{GLS}(x_{min}, Q^2)\Big|_{NLO} = S_{GLS}(Q^2)\Big|_{NLO} - \int_0^{x_{min}} \frac{dx}{x}\left[F_3^{NS}(x_0, t_0)\left(\frac{x}{x_0}\right)^{(1-bt)} \exp\left\{\int_{t_0}^{t}\left(\frac{\alpha(t)}{2\pi}\right)_{NLO} P(x_0, t)dt + \int_{t_0}^{t}\left(\frac{\alpha(t)}{2\pi}\right)^2_{NLO} Q(x_0, t)dt\right\}\right] \quad (7.16)$$

and

$$S_{GLS}(x_{min}, Q^2)\Big|_{NNLO} = S_{GLS}(Q^2)\Big|_{NNLO} - \int_0^{x_{min}} \frac{dx}{x}\left[F_3^{NS}(x_0, t_0)\left(\frac{x}{x_0}\right)^{(1-bt)} \exp\left\{\int_{t_0}^{t}\left(\frac{\alpha(t)}{2\pi}\right)_{NNLO} P(x_0, t)dt + \int_{t_0}^{t}\left(\frac{\alpha(t)}{2\pi}\right)^2_{NNLO} Q(x_0, t)dt + \int_{t_0}^{t}\left(\frac{\alpha(t)}{2\pi}\right)^3_{NNLO} R(x_0, t)dt\right\}\right] \quad (7.17)$$

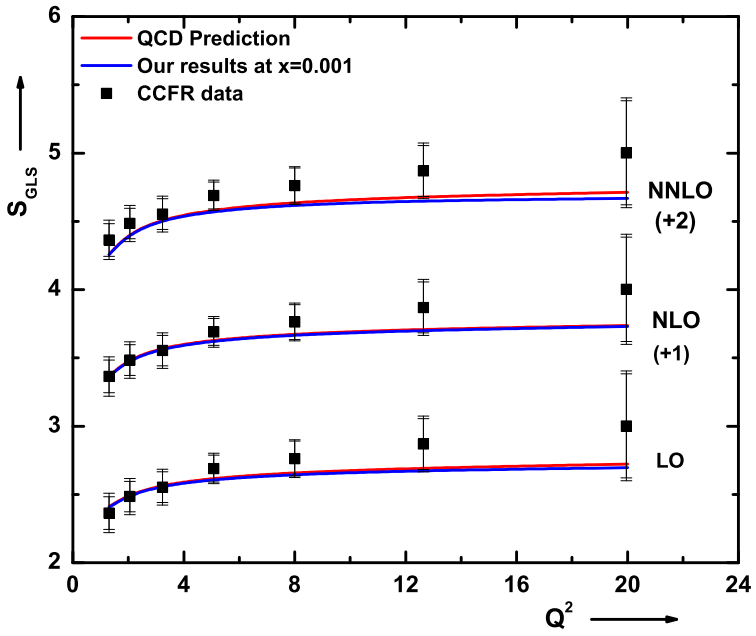

Figure 7.5: Results for the Gross - Llewellyn Smith sum rule at LO, NLO and NNLO, as a function of Q^2. The data are from the CCFR experiment [67]. The LO, NLO and NNLO curves are offset by the amount given in parenthesis. (Q^2's are taken in the unit of GeV^2).

respectively. Considering the input point, $xF_3(x_0 = 0.025, t_0 = 3.2GeV^2) = 0.3298$ from CCFR data we have calculated the GLS sum rule with QCD corrections up to NNLO using the expressions (7.15), (7.16) and (7.17) respectively and the results are depicted in Fig. 7.5, Fig. 7.6 and Fig. 7.7.

The Q^2 dependence of GLS integral as obtained from Eqs.(7.15), (7.16) and (7.17) are depicted in Fig. 7.6 in comparison with the experimental data taken from CCFR collaborations and the corresponding perturbative QCD predictions Eq.(7.12) in LO, NLO and NNLO. Here the inner error bar shows statistical errors and the outer one, a combination of statistical and systematic errors associated with CCFR data. Our results for LO, NLO and NNLO are represented by solid curves with the corresponding dashed curves representing theoretical QCD predictions Eq.(7.12) using higher-order QCD corrections (LO, NLO and NNLO) from [39]. Fig. 7.6 reflects the comparative picture of our NNLO results with those of CCFR data and theoretical predictions of QCD at NNLO and results obtained by Kataev and Sidorov(KS) in Ref. [167]. In Fig. 7.7 our results of GLSSR are plotted as a function of x_{min} in comparison with CCFR measurements. Here the uncertainties due to the chosen input is also estimated and

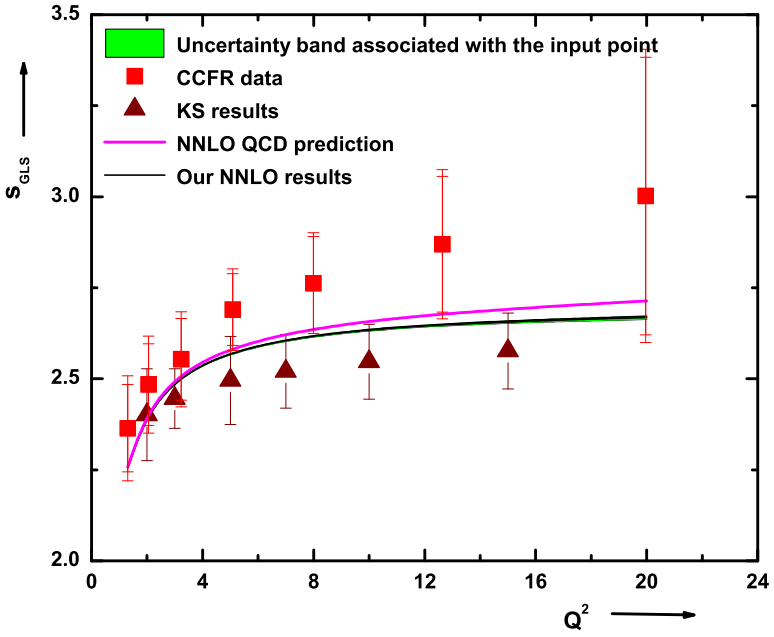

Figure 7.6: Our NNLO results for the Gross-Llewellyn Smith sum rule, for various values of Q^2, along with QCD predictions Eq.(7.12) in NNLO, in comparison with CCFR experiment [67]. The results with up triangle symbols along with uncertainty bars are the KS[167] results. (Q^2's are taken in the unit of GeV^2).

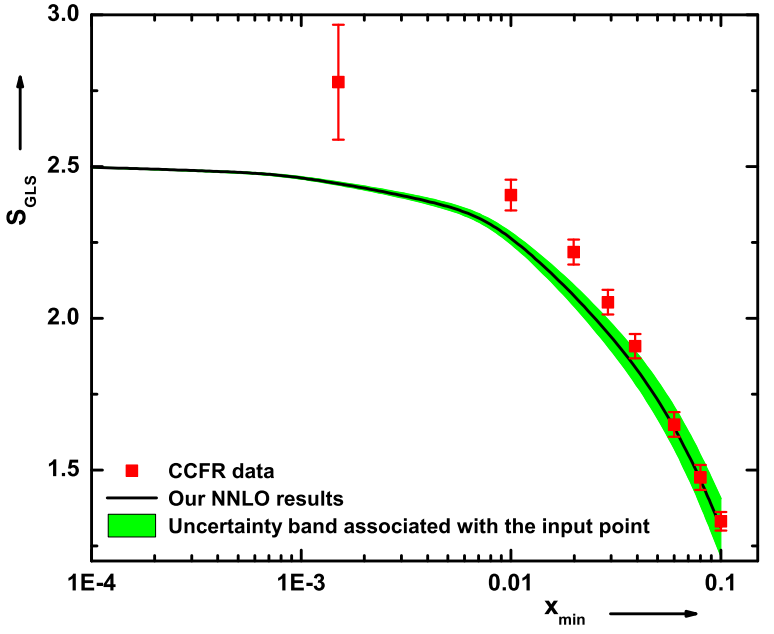

Figure 7.7: Results for the Gross-Llewellyn Smith sum rule, for various values of x. The data are taken from the CCFR experiment [67].

they are shown by the green band. From these figures one can see that our LO, NLO and NNLO results are within the statistical uncertainties of measurements by CCFR collaboration and also consistent with QCD predictions as well as KS results.

7.5 Determination of Bjorken Sum Rule

The Bjorken sum rule is associated with the spin dependent non-singlet structure function $xg_1^{NS}(x,Q^2)$. BSR relates the difference of proton and neutron structure functions integrated over all possible values of Bjorken variable, x to the nucleon axial charge g_A. At infinite four-momentum transfer squared, Q^2, the sum rule reads

$$S_{BSR} = \int_0^1 \frac{dx}{x} x g_1^{NS}(x,Q^2) = \frac{g_A}{6}. \tag{7.18}$$

In accord with QCD prediction, the leading twist pQCD correction up to NNLO for BSR is expressed as follows :

$$S_{BSR}(Q^2) = \int_0^1 \frac{dx}{x} x g_1^{NS}(x,Q^2) = \frac{g_A}{6}\left[1 - \frac{\alpha_s}{\pi} - 3.583\left(\frac{\alpha_s}{\pi}\right)^2 - 20.215\left(\frac{\alpha_s}{\pi}\right)^3\right], \tag{7.19}$$

which can be resolved to have

$$S_{BSR}(x_{min},Q^2) = \int_{x_{min}}^1 \frac{x g_1^{NS}(x,Q^2)}{x} dx = S_1^{p-n}(Q^2 - \int_0^{x_{min}} \frac{x g_1^{NS}(x,Q^2)}{x} dx. \tag{7.20}$$

Using the solutions of DGLAP equations, obtained in chapter 6, which provide well description of the small-x behaviour of $xg_1^{NS}(x,Q^2)$ structure function we can determine the integral on l.h.s. of Eq. 7.20, which will tend to represent the BSR for the limit $x = x_{min} \to 0$. Therefore, substituting (6.38),(6.39) and (6.40) in (7.20) and using the corresponding expressions for S_{BSR} in LO, NLO and NNLO, we obtain the Bjorken integral with LO, NLO and NNLO QCD corrections as

$$S_{BSR}(x_{min},Q^2)\Big|_{LO} = S_{BSR}(Q^2)\Big|_{LO} - \int_0^{x_{min}} \frac{dx}{x}\Bigg[g^{NS}(x_0,t_0) \left(\frac{x}{x_0}\right)^{(1-bt)} \exp\left\{\int_{t_0}^t \left(\frac{\alpha(t)}{2\pi}\right)_{LO} P(x_0,t)dt\right\}\Bigg], \tag{7.21}$$

$$S_{BSR}(x_{min},Q^2)\Big|_{NLO} = S_{BSR}(Q^2)\Big|_{NLO} - \int_0^{x_{min}} \frac{dx}{x}\Bigg[g^{NS}(x_0,t_0) \left(\frac{x}{x_0}\right)^{(1-bt)} \exp\Bigg\{\int_{t_0}^{t}\left(\frac{\alpha(t)}{2\pi}\right)_{NLO} P(x_0,t)dt + \int_{t_0}^{t}\left(\frac{\alpha(t)}{2\pi}\right)^2_{NLO} Q(x_0,t)dt\Bigg\}\Bigg] \tag{7.22}$$

and

$$S_{BSR}(x_{min},Q^2)\Big|_{NNLO} = S_{BSR}(Q^2)\Big|_{NNLO} - \int_0^{x_{min}} \frac{dx}{x}\Bigg[g^{NS}(x_0,t_0) \left(\frac{x}{x_0}\right)^{(1-bt)} \exp\Bigg\{\int_{t_0}^{t}\left(\frac{\alpha(t)}{2\pi}\right)_{NLO} P(x_0,t)dt + \int_{t_0}^{t}\left(\frac{\alpha(t)}{2\pi}\right)^2_{NLO} Q(x_0,t)dt\Bigg\}\Bigg] + \int_{t_0}^{t}\left(\frac{\alpha(t)}{2\pi}\right)^3_{NNLO} R(x_0,t)dt\Bigg\}\Bigg] \tag{7.23}$$

respectively. Considering a known input point $g^{NS}(x_0,t_0)$ from experimental data, we will be able to calculate the BSR integral up to NNLO corrections using the expressions, (7.21), (7.22) and (7.23) respectively. In our calculations we have used $g^{NS}(x_0 = 0.0143955, Q_0^2 = 5GeV^2) = 0.0133075$ as the input point, which is taken from the COMPASS[71] experimental data. With this input point we have calculated the Bjorken integral and the results in accord with equations (7.21), (7.22) and (7.23) are depicted in Fig. 7.8 and Fig. 7.9.

In Fig. 7.8, we have plotted our results for BSR integral in LO, NLO and NNLO as a function of low x limit of integration x_{min}, in comparison with COMPASS and HERMES measurements along with the results due to valon model(TSA)[131]. The uncertainties due to the parameter, b and the input point are estimated only for the NNLO results and as seen from the Fig. 7.8, they decrease with decrease in x_{min}. From Fig. 7.8 we observe an overall batter description of both COMPASS and HERMES data by our results with respect to the predictions due to valon model. Again our approach expects batter results for $x_{min} \to 0$, but there are no COMPASS measurement beyond $x \approx 0.004$ and HERMES measurement beyond $x \approx 0.02$ for our comparative analysis. Saturation of the COMPASS data for BSR is observed within $x > 0.004$, however available HERMES results have not saturated at $x \approx 0.01 - 0.02$.

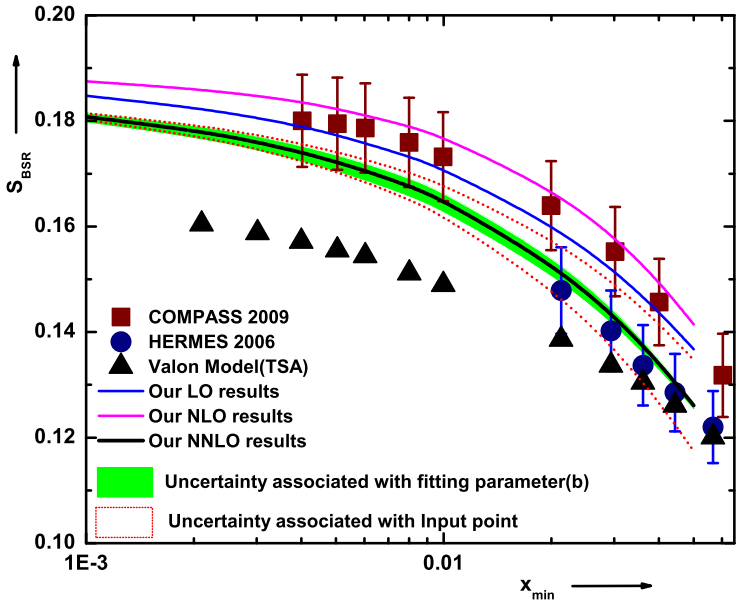

Figure 7.8: The results of Bjorken integral as a function of the low x limit of integration, x_{min}, in LO, NLO and NNLO in comparison with COMPASS [71] and HERMES[73] experimental data along with the predictions based on Valon model[131].

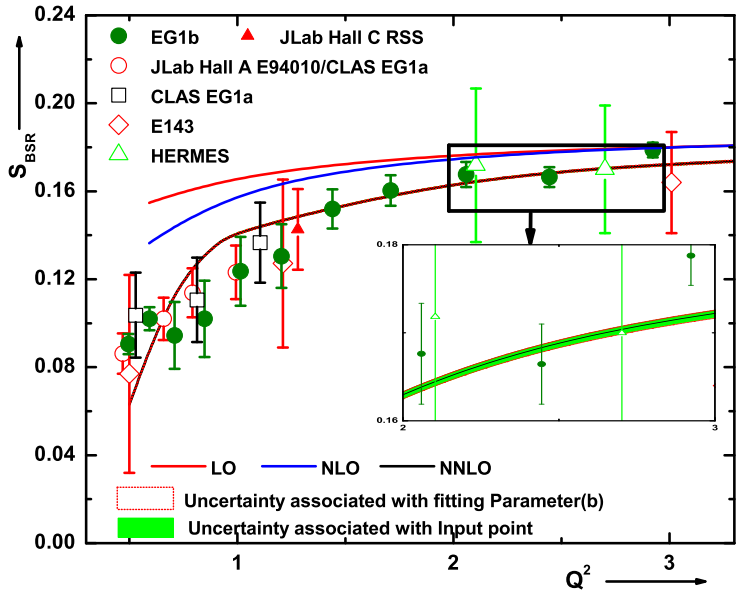

Figure 7.9: The results of Bjorken integral as a function of momentum transfer squared Q^2 in LO, NLO and NNLO against COMPASS [71] and HERMES[73] E143[75] and JLab [76–78] experimental data along with the theoretical as well as phenomenological analysis, Ref. [176–179]. (Q^2's are taken in the unit of GeV^2).

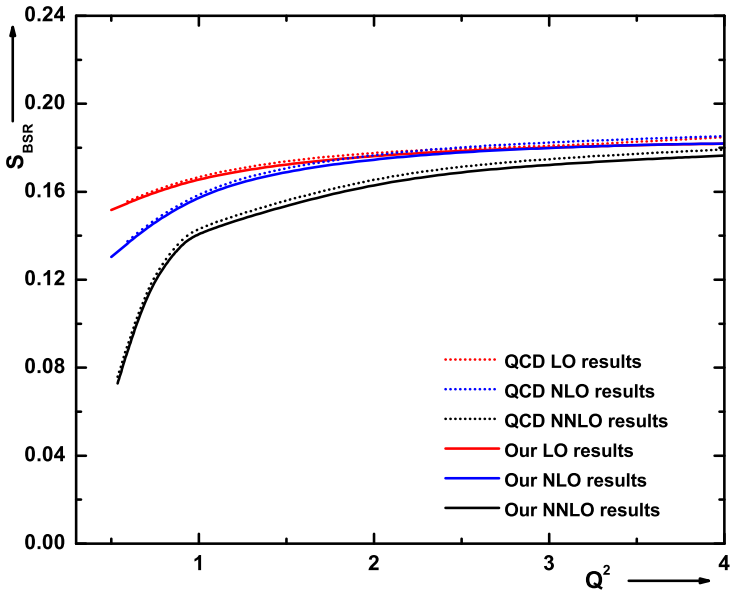

Figure 7.10: Our results of Bjorken integral in comparison with the QCD predictions up to NNLO[39]. (Q^2's are taken in the unit of GeV^2).

Thus we may expect to occur saturation within the smaller x region and within this region both HERMES and COMPASS results might agree with each other and reach an overall compatibility with our measurements.

The Q^2 dependency of Bjorken Sum Rule, as predicted by our expressions 7.21, 7.22 and 7.23 is depicted in Fig. 7.9. Here our results are compared with different experimental data taken from COMPASS [71], HERMES[73], E143[75] and JLab experiments [76–78] and with the theoretical as well as phenomenological analysis, Ref. [176–179]. The results depicted in this figure are calculated using the value of $\Lambda = 0.300GeV$. Here we have also estimated the uncertainty associated with the NNLO results due to the fitting parameter, b and the input point, and they are observed to be very small in this regard. It is also observed that the uncertainty decreases with decrease in Q^2.

In Fig. 7.10, we have compared our results with theoretical pQCD predictions (7.19) for Bjorken integral up to NNLO. Here our results are calculated with $\Lambda = 0.300GeV$. Within the estimated uncertainty our results show a very good consistency with those of pQCD predictions.

7.6 Summary

In the above sections we have presented some analytical expressions for the determination of the Gottfired sum rule, the Gross-Llewellyn Smith sum rule and the Bjorken sum rule. The expressions for sum rules are consisting of the solutions of the DGLAP evolution equations for F_2^{NS}, $xF_3(x,Q^2)$ and $xg_1^{NS}(x,Q^2)$ respectively, which are obtained in previous chapters, along with the input points $F_i^{NS}(x_0,t_0)$. Considering suitable input point as mentioned above, we have calculated the sum rule with pQCD corrections up to NNLO. We would like to emphasize that our results for various sum rules are in a overall good agreement with the corresponding experimental results as well as several strong theoretical, phenomenological predictions and also with the QCD predictions up to NNLO. These agreement, suggests that the Regge ansatz along with available data and QCD formalism allows to have a clean test of QCD predictions for various sum rule. □□